Supporting Information

Chemisorption of Pentacene on Pt(111) with a Little Molecular Distortion

Aldo Ugolotti,[*,†] Shashank S. Harivyasi,[‡] Anu Baby,[†] Marcos Dominguez,[¶,§] Anna Lisa Pinardi,[‖] Maria Francisca López,[‖] José Ángel Martín-Gago,[‖] Guido Fratesi,[⊥] Luca Floreano,[*,¶] and Gian Paolo Brivio[†]

†*Dipartimento di Scienze dei Materiali, Università degli Studi di Milano-Bicocca, via Cozzi 55, 20125, Milano, Italy*

‡*Institute of Solid State Physics, NAWI Graz, Graz University of Technology, Petersgasse 16, 8010 Graz, Austria*

¶*CNR-IOM, Laboratorio TASC, Basovizza SS-14, km 163.5, I-34149, Trieste, Italy*

§*Dipartimento di Fisica, Università degli Studi di Trieste, via Valerio 2, 34127, Trieste, Italy*

‖*Materials Science Factory, Instituto de Ciencia de Materiales de Madrid (ICMM-CSIC), Sor Juana Inés de la Cruz 3, E-28049 Madrid, Spain*

⊥*Dipartimento di Fisica, Università degli Studi di Milano, via Celoria 16, 20133, Milano, Italy*

E-mail: a.ugolotti@campus.unimib.it; floreano@iom.cnr.it

Adsorption energies and geometries for the tested configurations

We collect the complete set of results for all the configurations we have calculated, depicted in Figure S1. We highlight the most stable adsorption sites using bold fonts. We report adsorption energies in table S1, comparing the different vdW correction methods considered. The carbon atoms in the Pc molecule are divided into two roughly planar regions defined by the highest-lying and the lowest-lying C atom respectively, and separated by a distance Δz. The adsorption height z is then defined as the difference between averaged z coordinates of atoms in the lower region and the averaged z coordinates of the Pt atoms in the topmost layer. The adsorption height z and the distortion of molecular geometry Δz are collected in table S2, calculated with the vdW$_{surf}$ method. We report also the surface dipole induced by the molecule, labelled d. This last parameter is useful in getting a qualitative estimate for the charge transfer at an adsorption site other than the bri0 one: the lower the value of the dipole, compared to the one reported for the bri0 site, the lower the charge transferred. Finally in table S3 the effects on the adsorption geometry related to including different vdW correction schemes are reported.

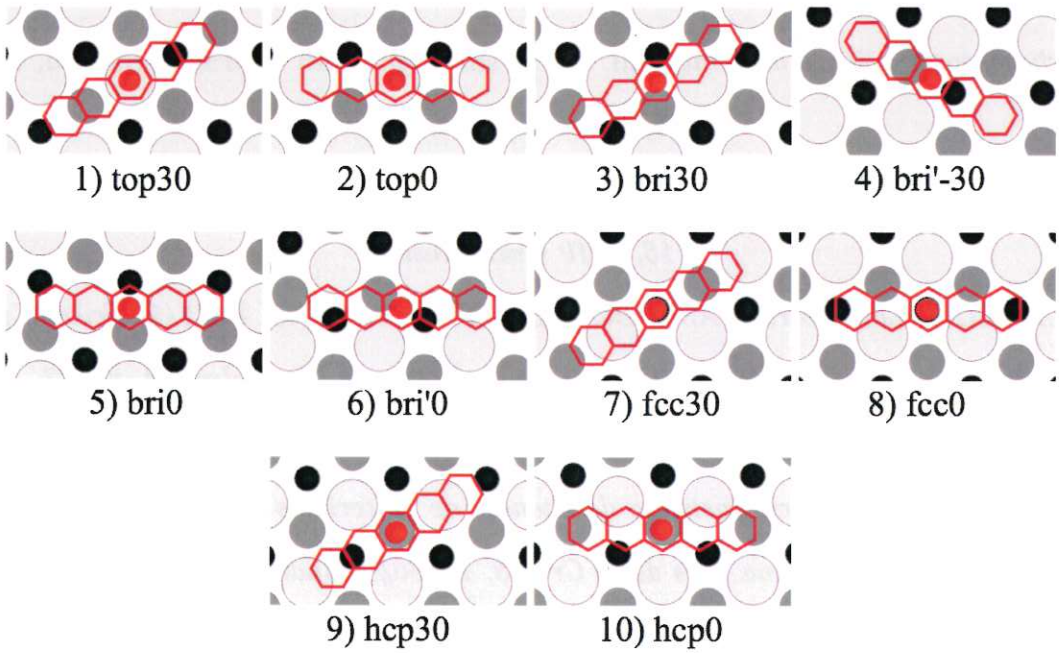

Figure S1: Cartoon of all the tested configurations. The molecule is represented in red (not to scale). All three layers of the Pt are shown: the smaller the circle (and darker the color) the deeper is the atom within the substrate.

Table S1: Adsorption Energy with Different vdW Schemes.

	E_{ads} (eV)			
Ads. site	PBE	D2	vdW_{surf}	vdW_{nl}
top30	1.53	10.28	6.13	5.40
top0	1.04	8.38	4.98	4.30
bri30	2.02	9.70	5.35	5.53
bri'-30	1.75	9.33	*	*
bri0	**3.13** (2.54)	**10.91**	**7.69** (6.65)	**7.38** (6.82)
bri'0	2.53	9.84	6.36	5.47
fcc30	1.41	9.09	5.50	5.01
fcc0	2.49	10.32	6.74 (5.82)	5.79 (5.48)
hcp30	1.58	9.11	5.62	5.04
hcp0	2.50	10.35	6.73	5.80

* relaxed into the bri30 configuration

The results for the six-layer slab are reported between brackets.

Table S2: Relaxed Adsorption Geometries.

	vdW_{surf}		
Ads. site	z (Å)	Δz (Å)	d (eÅ)
top30	2.0	0.7	1.7
top0	2.0	1.4	1.6
bri30	2.0	0.6	1.8
bri'-30	*	*	*
bri0	**2.1**	**0.2**	**2.1**
bri'0	2.1	0.1	2.1
fcc30	1.9	0.8	1.7
fcc0	1.9	0.8	1.8
hcp30	1.9	0.8	1.8
hcp0	2.0	0.7	1.8

* relaxed into the bri30 configuration

Table S3: Comparison of vdW Schemes in Calculating the Adsorption Energies and Geometries for bri0 site[i].

	E_{ads} (eV)	z (Å)	Δz (Å)	d (eÅ)
PBE	3.13 (2.54)	2.0 (1.9)	0.2 (0.3)	1.2 (2.1)
D2	10.91	2.0	0.2	2.1
vdW_{nl}	7.38 (6.82)	2.0 (1.9)	0.2 (0.3)	2.1 (2.1)
vdW_{surf}	7.69 (6.65)	2.1 (1.9)	0.2 (0.3)	2.1 (2.1)

[i] The results for the six-layer slab are reported between brackets.

Surface buckling

In figure S2, we show the displacement of the Pt atoms in the first layer for the fcc0 site, as a percentage of the bulk Pt distance. The rippling normal to the surface is strongly coupled to the molecular footprint in the z direction, where the Pt atoms underneath are lowered with respect to the clean surface, while those in correspondence of the molecular rim are lifted from the substrate. The in-plane atomic displacement is much smaller and results from the balance between the coupling of the molecule to the first surface layer (that is symmetric with respect to the short and long molecular axis) and the surface to subsurface Pt coupling (that is asymmetric with respect to the molecular axis due to the fcc layer stacking).

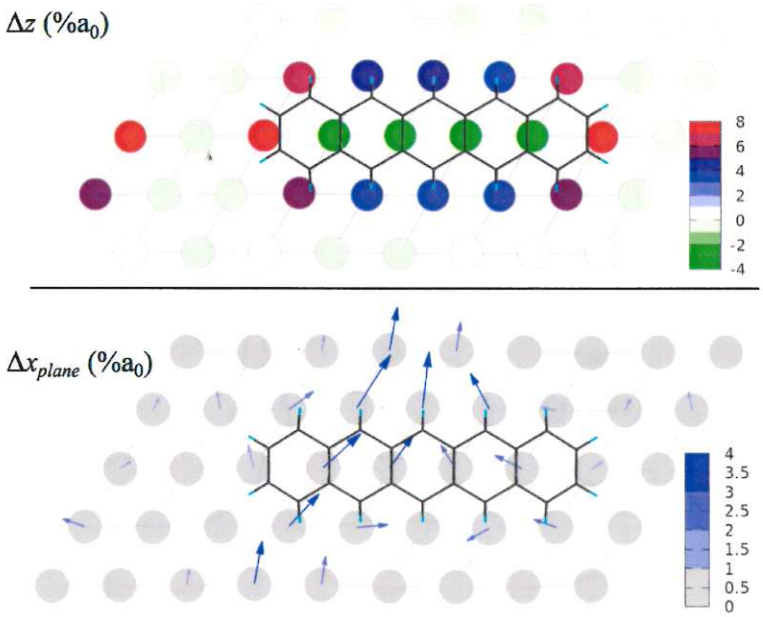

Figure S2: Displacements of the Pt atoms of the first layer with respect to the bulk lattice size a_0, calculated at the bri0 configuration. The vertical displacement is shown in the upper panel, where the different colours of the atom correspond to different amount of displacement. The in-plane displacement is shown in the lower panel, where the arrows indicate the direction and their length and colour correspond to the displacement amount.

Density of States projected onto Molecular Orbitals

To further investigate the electronic properties of the system, we calculated its density of states (DOS) and its projection onto the orbitals of the Pc in gas phase (MOPDOS), as shown in figure S3. The molecular layer displays a metallic DOS with non-resolved contributions. We report also the individual weight of selected gas phase orbitals to the total MOPDOS: the complex energy profile that suggests the formation of bonding-antibonding states due to the hybridization of the Pc orbitals with the bands of the metal. A similar coupling has already been observed with Al(001)[1] and copper surfaces,[2,3] but not to this extent.

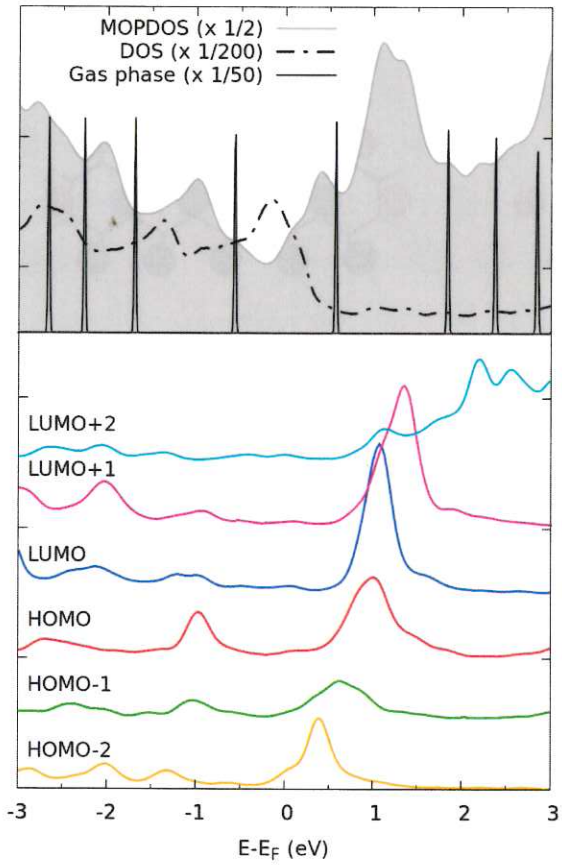

Figure S3: DOS/MOPDOS at the bri0 site, calculated for vdW$_{surf}$. The lower panel shows the weight of selected gas phase MO with respect to the total MOPDOS on the molecule.

Simulated STM and XPS for the second most stable adsorption configuration

In figures S4,S5 we report the simulated STM images and XPS spectrum for the second most stable configuration, namely the fcc0. Both results do not agree with the experiments.

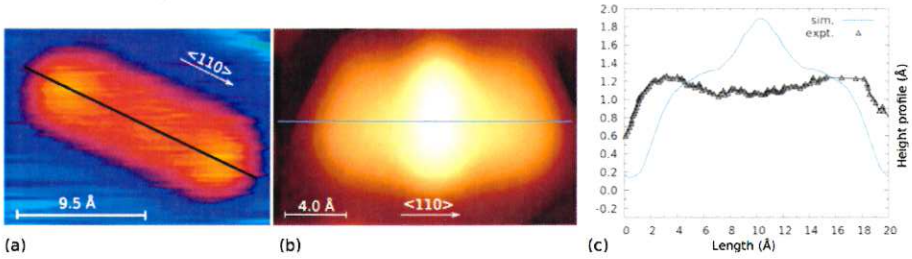

Figure S4: STM high-resolution experimental image (a) and height profile (c) (0.5 V sample bias and 0.396 nA tunneling current). In panel b) and c) the simulated results are reported for the fcc0 site.

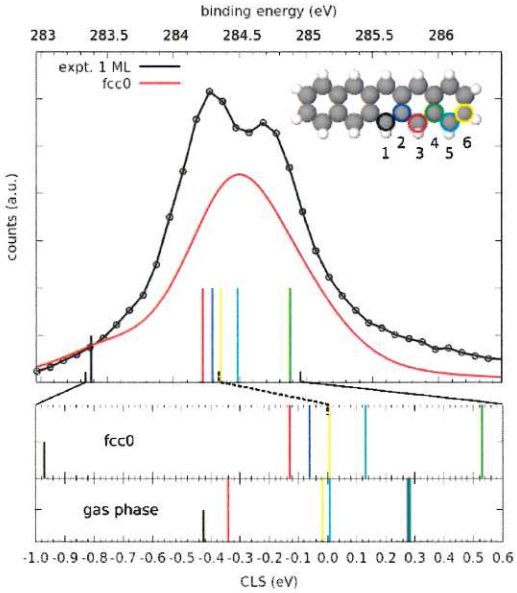

Figure S5: Comparison between the experimental C1 photoemission spectrum (line and markers) and the simulated one for the fcc0 site (full red line). The binding energy calculated for the inequivalent carbon atoms are also shown at the bottom of the graphic. In the zoomed energy range, we show the comparison between the core level shifts of the fcc0 adsorbed species (top) and the gas phase one (bottom).

NEXAFS atom-dependent components

The simulated NEXAFS spectra calculated in the bri0 site for each inequivalent C atom, reported in figure S6, show a small anisotropy in X and Y intensities, whereas their shape is similar. Such an azimuthal dichroism is similar to what has been observed in the case of the Al substrate.[4]

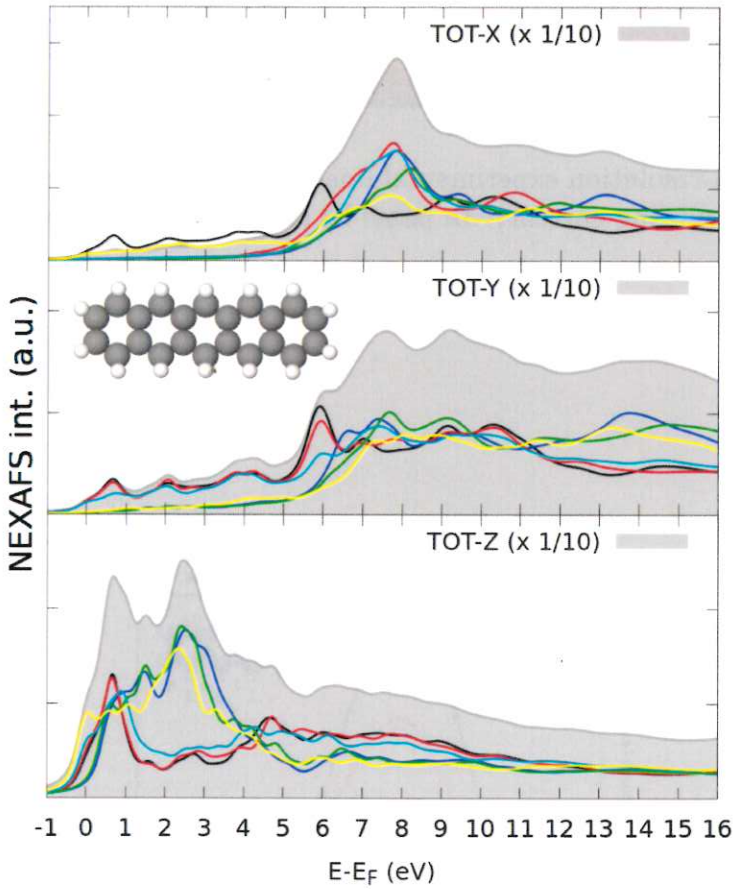

Figure S6: simulated NEXAFS spectrum for the bri0 configuration, showing the contributions from all inequivalent C atoms, along the three directions.

Coverage and Temperature dependent effects

The coverage dependence of XPS and NEXAFS, as well as the effect of mild temperature annealing is shown in figure S7. XPS spectra on as deposited films at RT display the presence of a weak shoulder at a binding energy of ~286 eV. The shoulder is observed in the sub-monolayer range (up to 1 ML) and disappears after annealing to 130°C together with the weak oxygen peak that appears just after pentacene deposition. This is indicative of the initial sticking of a minor amount of carbon monoxide produced by the heating filament of the Pc crucible. The XPS spectrum for 1 ML deposited at room temperature, RT, displays

a relatively much larger intensity of the main peak at 284 eV with respect to the 284.5 eV one. This extra intensity is due to residual 2nd layer molecules (that are also observed in STM images at ~1ML), which are easily desorbed by mild annealing at 130°C.

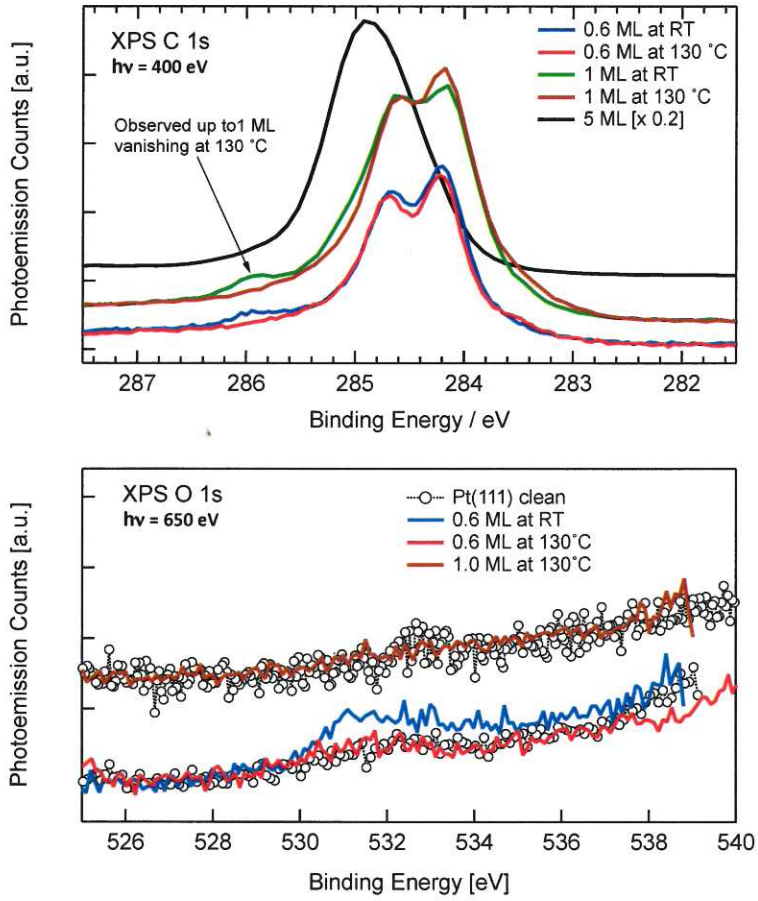

Figure S7: Comparison of C 1s (top panel) and O 1s (bottom) photoemission spectra measured by varying the deposition conditions, namely different coverages (0.6 to 5 monolayers) and annealing temperatures. The carbon shoulder at 286 eV vanishes together with the weak O 1s contribution at 531 eV by mild annealing to 400 K. No oxygen is present on the surface before deposition. For better comparison, each set of spectra has been vertically offset.

The presence at RT of 2nd layer molecules at the nominal coverage of 1 ML is more evident in NEXAFS spectra due to the much sharper spectral features of gas-phase-like molecules. From the comparison shown in Figure S8 between films measured at 1 and 5 ML, we can easily recognize the contribution of 2nd layer molecules in the pre-edge region at ~284 and in between the two main features of the adsorbed monolayer at ~286 eV, which correspond to contributions from LUMO and LUMO+1 resonances, respectively. Also in this case, these 2nd layer features disappear upon mild annealing to 130°C. The remaining asymmetry of the LUMO resonance at 1 ML, might be equally ascribed to residual 2nd layer molecule or to a minority of shorter acenes, as observed by STM.

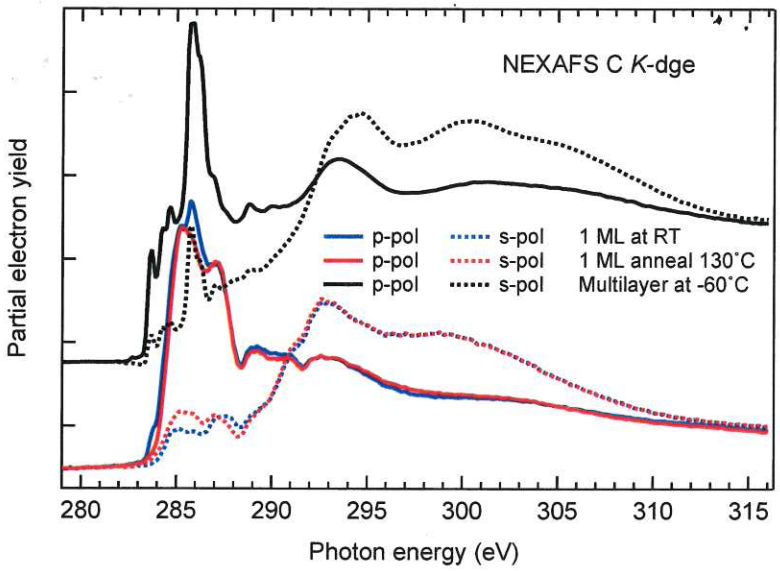

Figure S8: The C K-edge NEXAFS spectra measured at 1 ML before and after annealing to 400 K are shown in comparison with a spectrum measured at 5 ML. The LUMO and LUMO+1 contribution of 2nd layer molecules can be easily recognised in the as deposited monolayer spectrum at 284 and 286 eV, respectively. Most of 2nd layer molecules are desorbed at 400 K.

References

(1) Baby, A.; Lin, H.; Brivio, G. P.; Floreano, L.; Fratesi, G. Core-level spectra and molecular deformation in adsorption : V-shaped pentacene on Al (001). Beilstein J. Nanotechnol. **2015**, 6, 2242–2251.

(2) Ferretti, A.; Baldacchini, C.; Calzolari, A.; Di Felice, R.; Ruini, A.; Molinari, E.; Betti, M. G. Mixing of electronic states in pentacene adsorption on copper. Phys. Rev. Lett. **2007**, 99, 1–4.

(3) Shi, X. Q.; Li, Y.; Van Hove, M. A.; Zhang, R. Q. Interactions between organics and metal surfaces in the intermediate regime between physisorption and chemisorption. J. Phys. Chem. C **2012**, 116, 23603–23607.

(4) Baby, A.; Fratesi, G.; Vaidya, S. R.; Patera, L. L.; Africh, C.; Floreano, L.; Brivio, G. P. Anchoring and bending of pentacene on aluminum (001). J. Phys. Chem. C **2015**, 119, 3624–3633.